

Quantitative four-dimensional tracking of cytoplasmic and nuclear HIV-1 complexes

Nathalie Arhel^{1,6}, Auguste Genovesio^{2,4,6}, Kyeong-Ae Kim⁵, Sarah Miko¹, Emmanuelle Perret³, Jean-Christophe Olivo-Marin², Spencer Shorte³ & Pierre Charneau¹

Emerging real-time techniques for imaging viral infections provide powerful tools for understanding the dynamics of virus-host cell interactions. Here we labeled human immunodeficiency virus-1 (HIV-1) integrase with a small tetracycline tag, which preserved the virus' infectivity while allowing it to be labeled with the bis-arsenical fluorescein derivative FLAsH. This labeling allowed us to image both intracytoplasmic and intranuclear HIV-1 complexes in three dimensions over time (4D) in human cells and enabled us to analyze HIV-1 kinetics by automated 4D quantitative particle tracking. In the cytoplasm, HIV-1 complexes underwent directed movements toward the nuclear compartment, kinetically characteristic of both microtubule- and actin-dependent transport. The complexes then adopted smaller movements in a very confined volume once associated with the nuclear membrane and more diffuse movements once inside the nucleus. This work contributes new insight into the various movements of HIV-1 complexes within infected cells and provides a useful tool for the study of virus-host cell interactions during infection.

The dynamic imaging of single viruses within living cells is fundamental to a better understanding of virus-host cell interactions. Important breakthroughs in understanding the intracellular dynamic behaviors of these viruses have been brought about by conjugating their outer capsid proteins to a fluorophore, as with adenovirus¹, adeno-associated virus² and simian virus 40 (ref. 3); labeling the outer envelope with fluorescent lipophilic dyes, as with influenza virus⁴; or labeling the actin tails of vaccinia virus with green fluorescent protein (GFP)⁵. In the case of HIV-1, tagging of viral protein R (Vpr) with GFP permitted the first observation of intracellular HIV-1 complexes in living cells and implicated the microtubule network in cytoplasmic routing⁶. In the first 2 h after infection, GFP-labeled HIV-1 complexes were shown to move in curvilinear paths along microtubules towards the perinuclear area. These GFP-tagged HIV-1 particles also proved useful for studying budding and cell-to-cell transmission⁷. Recently, the incorporation of Gag-GFP⁸ and Gag-tetracycline⁹ in HIV-1 virions has also been

reported. However, despite these advances, many steps of the HIV-1 replication cycle—such as intranuclear events—remain inaccessible. In addition, the use of large labels and modifications in HIV-1 *gag* or *pol* frequently lead to disruption of viral functions and marked loss of infectivity^{8,10}.

The directional transport of intracellular particles such as vesicles or viruses is ensured, to varying extents, by the microtubule and actin filament cytoplasmic networks. Transport along microtubules is reportedly saltatory, with transport over distances of $\sim 10 \mu\text{m}$ at velocities of $\sim 1 \mu\text{m/s}$ (refs. 11,12). Time-lapse analyses of microtubule-dependent movements of viral particles such as vaccinia virus¹³, adenovirus^{1,14} or influenza virus⁴ revealed maximum speeds ranging from ~ 0.2 to $2 \mu\text{m/s}$. Myosin-directed actin-based transport, which is distinct from the propulsion on actin filaments described for some intracellular bacteria and vaccinia virus, tends to be substantially slower than microtubule-directed transport ($\sim 0.1 \mu\text{m/s}$) and covers shorter distances^{4,11,12}.

Here we report the labeling of infectious HIV-1 viruses with the bis-arsenical fluorescein derivative FLAsH after tagging of the viral integrase protein with a tetracycline tag. This technique enabled the real-time imaging of the entire postfusion early phase of the HIV-1 replication cycle, revealing previously unexplored aspects of viral intracellular movements. We also introduce a reliable quantitative method that allows for the first time the 4D tracking of HIV-1 complexes and the assignment of precise kinetic parameters for the various observed intracellular movements. We found that cytoplasmic HIV-1 complexes adopted directed movements toward the nuclear compartment, which are kinetically characteristic of both microtubule- and actin-dependent transport. Initial movements from the cell periphery toward the nucleus were characteristic of microtubule-directed transport, whereas movements occurring in the area directly around the nucleus were consistently slower and shorter-ranging, a characteristic compatible with actin-directed transport. We also provide the kinetic characteristics of HIV-1 complexes associated with the nuclear membrane and within the nuclear compartment.

¹Groupe de Virologie Moléculaire et Vectorologie, ²Unité d'Analyse d'Images Quantitative and ³Centre d'Imagerie Dynamique, Institut Pasteur, 25-28 rue du Dr. Roux, 75724 Paris, France. ⁴SIP-CRIP5 Université Paris V, 45 rue des Saints Pères, 75006 Paris, France. ⁵Institut Pasteur Korea, 39-1, Hawolgok-dong, Sungbuk-gu, Seoul, Korea. ⁶These authors contributed equally to this work. Correspondence should be addressed to P.C. (charneau@pasteur.fr) or J.-C.O.-M. (jcolivo@pasteur.fr).

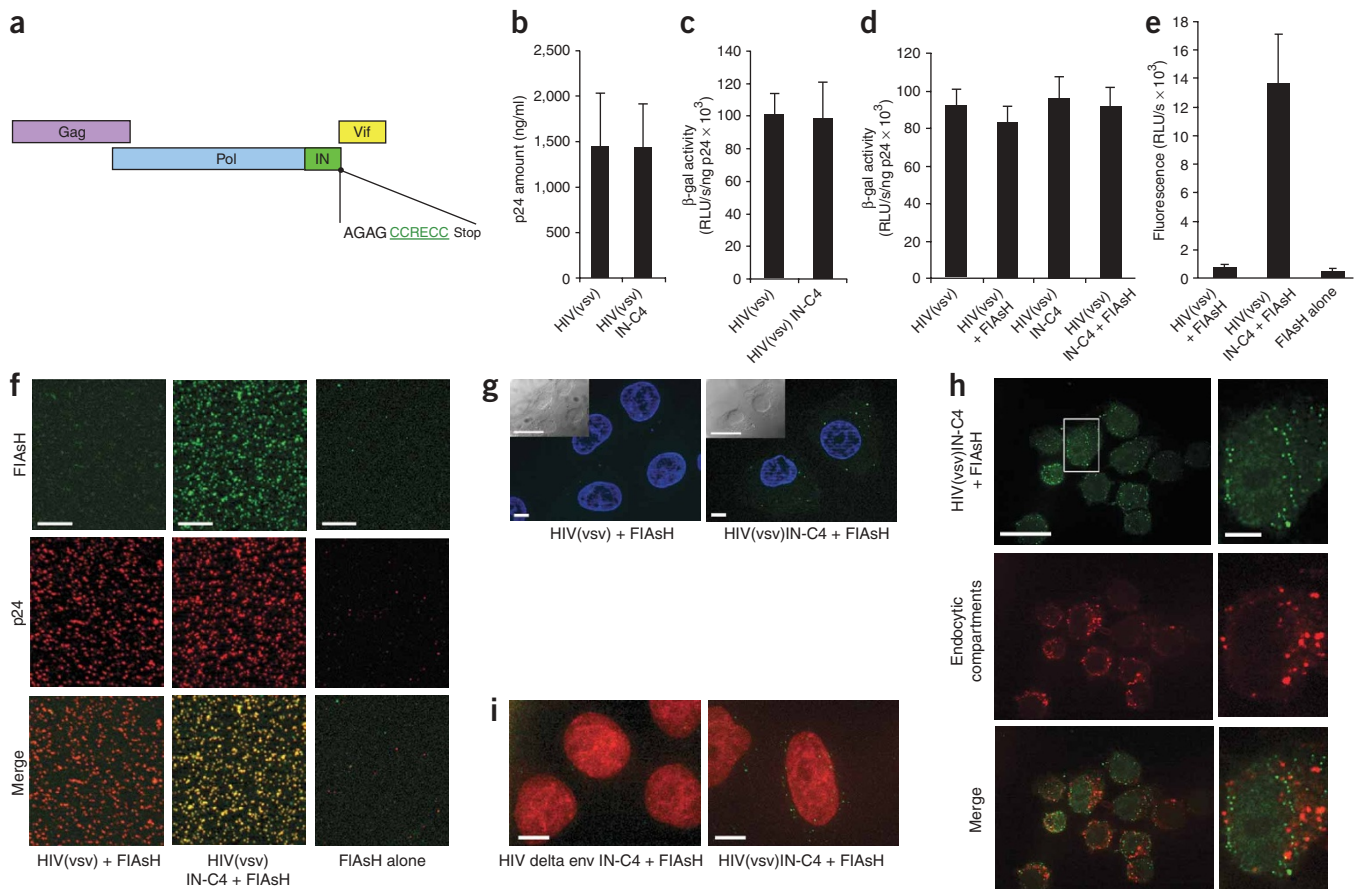


Figure 1 | Fusion of a tetracycline tag C-terminal of HIV-1 integrase (IN) does not perturb viral functions and permits highly specific labeling of integrase by FAsH. **(a)** Schematic representation of the viral construct. **(b)** Tag insertion does not perturb virus production. Data represent mean \pm SD of three independent experiments. **(c,d)** Neither tag insertion **(c)** nor FAsH labeling **(d)** perturb viral infectivity. Data shown represent mean \pm SD of three independent experiments carried out in triplicate. RLU, relative light units. **(e)** Highly specific labeling of tetracycline-tagged HIV-1 particles by FAsH. Viruses were normalized at 500 ng of p24. Fluorescence was measured at 485–570 nm. Data shown represent mean \pm SD of three independent experiments. **(f)** FAsH-labeled particles colocalize with p24 capsid labeling. Colocalization analysis by wavelet filtering¹⁷ revealed that 77% of p24-positive viral particles colocalized with FAsH labeling, indicating high labeling efficiency of viruses. The ultracentrifugation step led to some aggregation of particles, inducing apparent heterogeneity in particle size. **(g)** Residual nonspecific FAsH induces minimal background fluorescence 24 h after infection compared with specific viral labeling. Viruses were normalized at 120 ng of p24. Insets, Nomarski interference contrast images of the same field. **(h)** Minimal colocalization of labeled viruses with acidic compartments 6 h after infection indicates that viruses have already fused into the cytoplasm. **(i)** Envelope-minus ('delta env') HIV-1 cannot enter the cytoplasm by fusion. Cells were infected with FAsH-labeled envelope-minus and VSV-G–pseudotyped HIV-1 viruses and observed 6 h after infection. All scale bars indicate 5 μ m, except for insets of **g** and left images of **h**, where they indicate 20 μ m.

RESULTS

Insertion of a tetracycline tag C-terminal of HIV-1 integrase

We inserted a small tetracycline tag (CCRECC) C-terminal of HIV-1 integrase (Fig. 1a) for high-affinity labeling by FAsH¹⁵. Cells transfected with wild-type or tagged proviral clones, to monitor steps from transcription to assembly and budding, produced equal amounts of viral particles (Fig. 1b). In addition, one-round titration assays in our P4 indicator cell line, which encompass early steps from entry to *tat* activation, revealed no differences in the infectivity of wild-type and tagged particles (Fig. 1c). The tagged particles retained wild-type infectivity after labeling with FAsH ligand (Fig. 1d). Therefore, fusion of the tetracycline tag C-terminal of integrase did not lead to a loss in infectivity in either early or late steps of the replication cycle, and labeling with the FAsH ligand did not interfere with the normal functions of the virus.

Labeling of tetracycline-tagged HIV-1 particles with FAsH

Our experimental approach of labeling viral particles *in vitro* before infection resulted in increased specificity of labeling and reduced background noise and toxicity linked to the use of reducing agents required for labeling within living cells. Labeling of wild-type HIV-1 viruses proved very efficient, and the viruses retained infectivity (data not shown). However, vesicular stomatitis virus (VSV)-G–pseudotyped HIV-1 is more stable and naturally more infectious. We therefore used this virus for the full recovery of viral infectivity after the ultracentrifugation step required to remove unbound FAsH. This virus also allows greater multiplicities of infection, enabling the tracking of numerous trajectories within a single cell.

We focused our analyses on routing to the nucleus and intranuclear movements, bypassing the fusion and immediate postentry events although these are directly accessible by tagging particles with native HIV-1 envelope. Virus particles containing

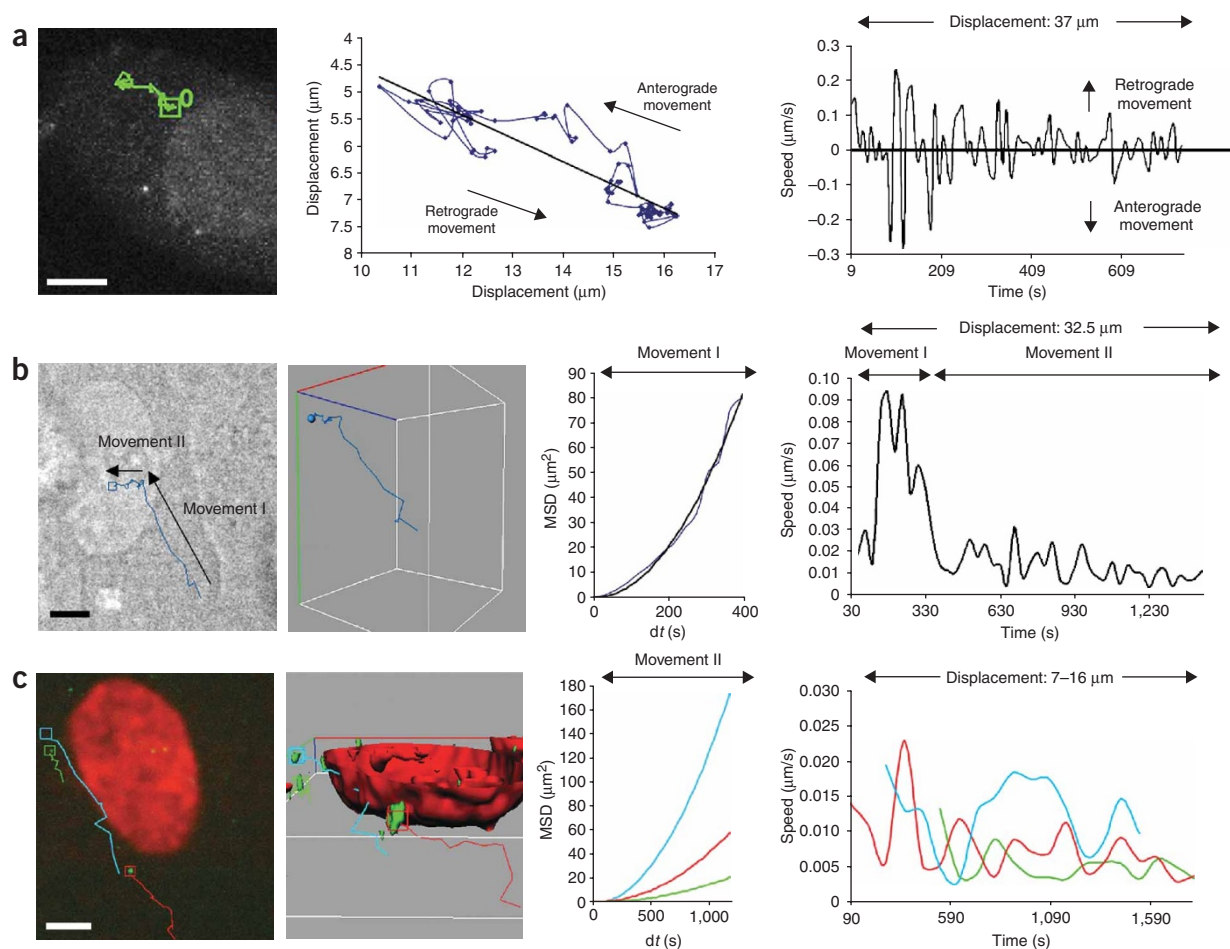


Figure 2 | Automated 4D tracking analysis of cytoplasmic FIAsh-labeled HIV-1 complexes allows the distinction between microtubule-like and actin-like directed movements. We observed P4 cells between 1 and 20 h after infection with FIAsh-labeled HIV_{LAI}(vsv)IN-C4 virus. Image stacks ($z = 0.3\text{--}0.8\ \mu\text{m}$) were acquired at 8-, 30- and 90-s intervals for 12, 24 and 32 min, respectively, for **a–c**. Scale bars, 5 μm . Nuclei are labeled with H2B-mRFP in **c**. Images show 2D and 3D representations of trajectories. **(a)** Fast microtubule-like movement is saltatory and both retrograde and anterograde, with an overall directionality toward the nuclear compartment. **(b)** 4D tracking of an individual cytoplasmic HIV-1 complex reveals passage from microtubule-directed (I) to actin-like movements (II) at the vicinity of the nuclear compartment. MSD plot against time has an order-two polynomial fit, indicating directed movement. **(c)** 4D tracking of individual HIV-1 complexes close to the nuclear compartment with actin-directed movement parameters. Each trajectory is identified by a specific color. MSD plot indicates directed movements.

CCRECC-tagged integrase were specifically labeled by the FIAsh ligand with a 15- to 30-fold increase in overall fluorescence above control background levels (**Fig. 1e**). FIAsh-labeled virions appeared as brightly fluorescent subresolution particles by structured illumination fluorescence microscopy, and their viral nature was confirmed by strong colocalization with p24 capsid labeling (**Fig. 1f**).

FIAsh-labeled HIV-1 complexes were readily detectable within the cytoplasm of infected cells, and background cell-associated fluorescence resulting from interactions between residual FIAsh and endogenous cellular components was minimal (**Fig. 1g**). From 6 h after infection, intracellular viral complexes showed minimal (<10%) colocalization with acidified endocytic compartments (**Fig. 1h**), indicating that most VSV envelope-mediated fusion events from late endosomes, through which HIV complexes are released into the cytoplasm, occurred less than 6 h after infection. This is concordant with previous work indicating that 68% of total intracellular capsids are already cytosolic as early as 1 h after infection with VSV-G-pseudotyped HIV¹⁶. Moreover, infection

with HIV-1 particles lacking any envelope protein showed minimal background at 6 h after infection, indicating that HIV-1 virus without envelope protein cannot enter the cytoplasm by fusion (**Fig. 1i**). We therefore validated the use of FIAsh to label tetra-cysteine-tagged HIV-1 integrase for the detection of infectious HIV-1 complexes within living cells.

Characterization of HIV-1 cytoplasmic transport

After infection, we imaged individual intracellular FIAsh-labeled HIV-1 complexes in 4D using spinning-disk confocal microscopy. We developed a computer vision program for automated 4D tracking of fluorescent particles, which allowed the intracellular movements of HIV-1 to be quantified relative to the center of mass of the cell nucleus. This program enables the detection of HIV-1 complexes in image stacks using a 3D wavelet transform¹⁷. Tracking is performed within a bayesian framework that allows the prediction of a complex's new probable position based on its past positions and on realistic models of biological dynamics¹⁸.

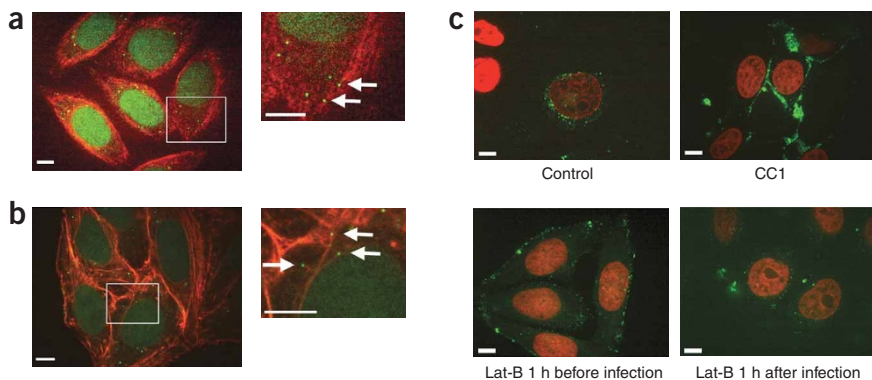


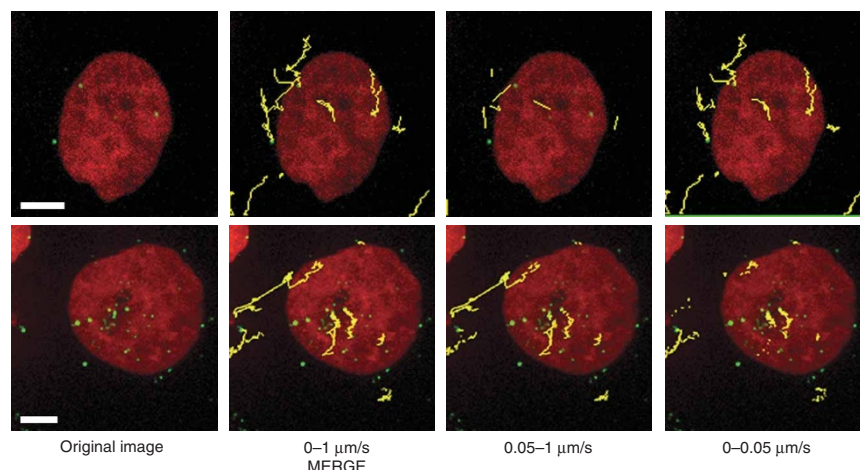
Figure 3 | FLAsH-labeled HIV-1 complexes colocalize with microtubules and actin filaments 6 h after infection. Right panels show enlargements of the boxed areas. Arrows point to HIV-1 complexes. (a) Microtubules were labeled with monoclonal antibody to α -tubulin and Cy3-conjugated anti-mouse secondary antibody. (b) Actin filaments were labeled with a phalloidin-TRITC conjugate. (c) Inhibition of microtubule- or actin-dependent transport in infected cells results in an inhibition of perinuclear accumulation of FLAsH-labeled virus 24 h after infection. Cells expressing mRFP-H2B were either transduced with TRIP-CC1 or treated with 200 nM latrunculin B (Lat-B) and then infected with FLAsH-labeled virus, or first infected and then treated with latrunculin B. Untreated cells were used as a control. All scale bars indicate 5 μ m.

We observed infected P4 cells between 4 and 24 h after infection and acquired image stacks at 5- to 90-s intervals. All calculations and analyses were carried out in 4D. We analyzed 923 trajectories of single HIV-1 intracellular complexes in 63 cells from six independent experiments. In particular, we focused on representative trajectories presented in this report.

At early time points after infection, cytoplasmic HIV-1 reverse-transcription complexes exhibited essentially two types of movements, whose parameters were compatible either with microtubule-directed movement^{1,4,6,13,14} or actin-mediated motility^{4,11,12}. Microtubule-directed movement (movement I) comprised curvilinear displacements as previously reported⁶, associated with long displacements, an average speed of 0.082 ± 0.0074 μ m/s (166 measurements) and peaks between 0.1 and 1 μ m/s. The movement was saltatory, both anterograde and retrograde, but with an overall directionality toward the nuclear compartment (Fig. 2a and Supplementary Video 1 online). The same movements suggestive of microtubule-directed transport were observed with HIV-1 particles carrying wild-type HIV-1 envelope (ref. 6 and data not shown).

Our observations also revealed a switch of single reverse-transcription complexes from the fast type of movement to slower movements, which would be more

Figure 4 | 2D representation of typical trajectories with gating according to maximal velocities. Original images show FLAsH-labeled HIV-1 complexes as they were located at the end of the acquisition, with nuclei in red. Scale bars indicate 5 μ m. Merged images show 2D representations of all trajectories adopted by HIV-1 complexes during the time of acquisition, superimposed on the original image. The total trajectories are gated according to maximum velocity (0.05–1 μ m/s for microtubule-like movements and 0–0.05 μ m/s for actin-like movements).



characteristic of actin-directed transport, when reaching the perinuclear area (11 independent observations of this transition; see example in Fig. 2b and Supplementary Video 2 online). This second type of movement (II) was also directional, as indicated by the order-two polynomial fit of the mean square displacement (MSD) plots, but with a slower average speed of 0.018 ± 0.0013 μ m/s (114 measurements) covering shorter distances and predominantly close to the nuclear compartment (Fig. 2c and Supplementary Video 3 online).

We precisely analyzed all acquired trajectories to extrapolate maximum velocities and total displacement of the HIV-1 complexes during the time of acquisition. Analysis of 421 trajectories that we acquired at early time points after infection with one stack acquisition every 10 s or less indicated that 296 (70%) had a maximum velocity >0.1 μ m/s, typical of microtubule-dependent movement (Supplementary

Fig. 1 online). For the slower actin-like movements, we analyzed 153 trajectories from independent series taken with one stack acquisition every 30 s and found that more than two thirds (117, or 76.5%) had a maximum speed between 0.025 and 0.05 μ m/s with the majority (24%) between 0.025 and 0.027 μ m/s (Supplementary Fig. 1). Finally, we calculated the total displacement of all 923 trajectories analyzed and found an overall broad distribution, with 742 HIV-1 complexes (80.4%) covering distances between 5 and 32.5 μ m during 30-min acquisitions (Supplementary Fig. 1).

The implication of microtubule- and actin-based movements, deduced on the basis of speed, trajectory and displacement of cytoplasmic complexes, was supported by colocalization studies using tubulin-specific antibody or a phalloidin-TRITC conjugate, suggesting that HIV-1 complexes colocalize with both microtubules (Fig. 3a), as previously shown⁶, and actin filaments (Fig. 3b). In addition, stable expression of the transdominant inhibitor p150^{217–548} CC1 domain of dynactin, which uncouples dynein-based transport¹⁹, inhibited transport of FLAsH-labeled virus to the nuclear compartment, with HIV-1 complexes

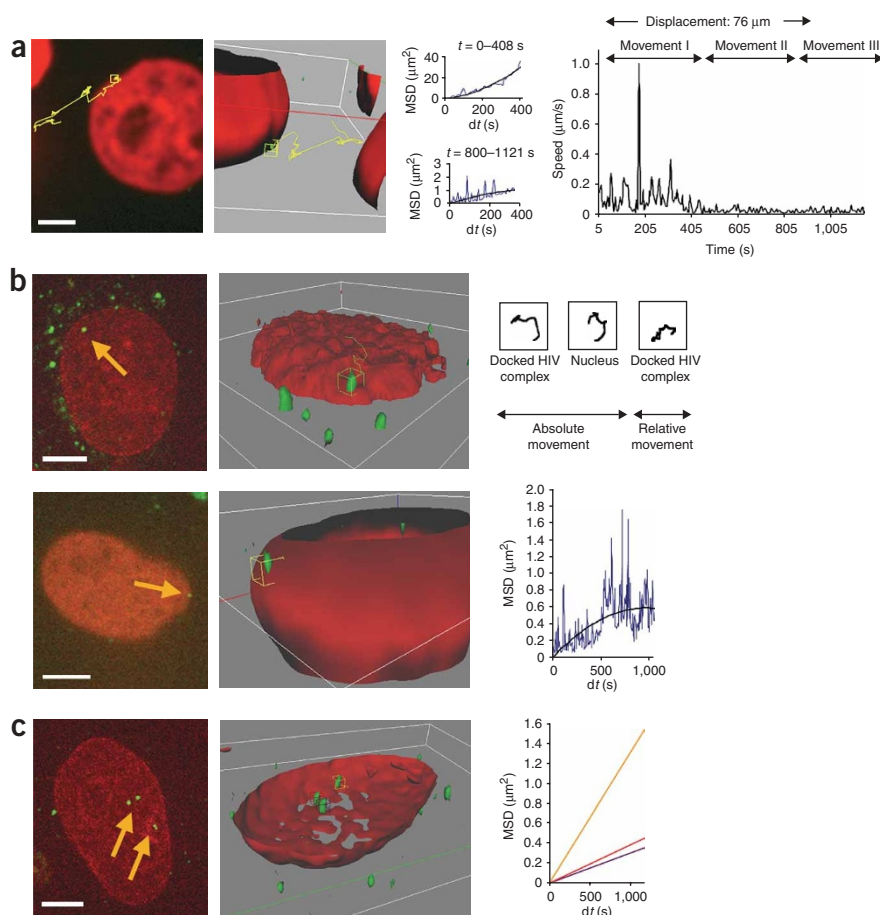


Figure 5 | FLAsH labeling of HIV-1 integrase allows detection and characterization of HIV-1 complexes docked at the nuclear membrane and within the nuclear compartment. P4 cells were observed between 20 and 24 h after infection with FLAsH-labeled HIV_{LAI}(vsv)IN-C4 virus. Image stacks ($z = 0.8 \mu\text{m}$) were acquired at 5-s intervals for **a** and **b** (bottom) and at 90-s intervals for **b** (top) and **c** for 21–32 min. All scale bars indicate $5 \mu\text{m}$. **(a)** 4D tracking of an individual HIV-1 complex reveals passage from movement I (with peaks up to $1 \mu\text{m/s}$) to II and finally to association with the nuclear membrane (movement III). MSD plots contrast initial directed movement (movement I; $t = 0\text{--}408 \text{ s}$) with restricted movement upon docking (movement III; $t = 800\text{--}1121 \text{ s}$). **(b)** Characterization of the movement of HIV-1 complexes at the nuclear membrane. Images show confocal slices and 3D surface reconstructions with individual docked HIV-1 complexes (arrows). As the nucleus moves over time, the relative movement of the docked complex was accurately calculated by subtracting the movement of the nucleus from that of the complex (top right panels). The MSD plot (bottom right) indicates confined movement within a volume of $0.7 \mu\text{m}$ average diameter. **(c)** Characterization of movement of HIV-1 complexes within the nucleoplasm of infected cells. Images show a confocal slice and 3D reconstruction with individual HIV-1 complexes within the nuclear compartment (arrows). Each line color refers to an individual intranuclear complex. MSD plots are linear in fit, indicating diffuse movement.

accumulating in the periphery of the cytoplasm (Fig. 3c). When latrunculin B, an inhibitor of actin-mediated transport, was added to cells before infection, cytoplasmic transport of viruses was severely impaired, with viruses accumulating at the plasma membrane (Fig. 3c). This is likely to be indicative of the previously described involvement of the actin filament network underlying the plasma membrane in the early steps of viral entry²⁰. On the other hand, when infection was allowed to proceed for 1 h before latrunculin B was added, viruses accumulated close to the nuclear compartment, albeit some distance away from the nuclear membrane (Fig. 3c), substantiating the existence after microtubule-directed movement of a viral actin-mediated transport close to the nuclear membrane and before docking.

To visualize the cellular distribution of microtubule- and actin-dependent movements, we spatially represented typical trajectories according to the maximal velocity at each measurement (Fig. 4). We represented all measured portions of each trajectory by gating maximum speeds either at $0\text{--}0.05 \mu\text{m/s}$ for actin-like movements or $0.05\text{--}1 \mu\text{m/s}$ for microtubule-like movements. The results confirmed that actin-like movements tend to predominate in the perinuclear region and that complexes associated with the nuclear membrane arrived there as a result of an actin-like trajectory.

Association of HIV-1 complexes with the nuclear membrane

After cytoplasmic transport, the labeled complexes eventually associated with the nuclear membrane, a step we refer to as ‘docking,’ although we have no evidence yet that this localization

at the nuclear membrane corresponds to an association with nuclear pores. We noted that all observed docking events were systematically preceded by slow actin-like mobility in the perinuclear area (25 independent observations of this transition; example given in Fig. 5a and Supplementary Video 4 online). We also found that cytoplasmic transport to the nuclear compartment was asynchronous and rapid (Fig. 5a), as previously shown^{6,21,22}, with complexes observed at the nuclear membrane as early as 6 h after infection. After compensating for the movement of the cell by subtracting the movement of the center of mass of the nucleus from that of individual HIV-1 complexes, we found that complexes at the nuclear membrane were very restricted in their displacements (Fig. 5b and Supplementary Video 3) and ‘vibrated’ within a confined volume with a mean speed of $0.018 \pm 0.0015 \mu\text{m/s}$ (100 measurements; movement III in Fig. 5a). The movement of docked particles can therefore be distinguished from movement II (which we suggest is actin-based) not on the basis of speed parameters, but rather on the type of movement, directed in the case of transport toward the nucleus and confined for docking at the nuclear membrane (Supplementary Video 5 online).

Visualization of intranuclear HIV-1 movements

In principle, labeling of integrase enables the indirect imaging of intracellular viral DNA until integration, as biochemical fractionation studies have shown that all integrase proteins in HIV-1 replicative complexes are stably associated with the viral DNA²³. We occasionally detected FLAsH-labeled HIV-1 complexes within

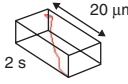
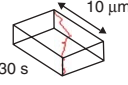
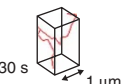
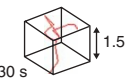
	Type	Velocity	3D tracks	Movement characteristics
Movement I	Microtubule-directed	Peaks at 0.1–1 $\mu\text{m/s}$		Directed
Movement II	Actin-directed	Under 0.03 $\mu\text{m/s}$		Directed
Movement III	Docking at the nuclear membrane	Under 0.03 $\mu\text{m/s}$		Confined
Movement IV	Intranuclear movement	Under 0.005 $\mu\text{m/s}$		Diffusive

Figure 6 | Summary of movements and kinetic characteristics of HIV-1 complexes observed within infected cells. Examples of tracks are represented in 3D. Space and time scales are given for each movement type.

the nuclear compartment 24 h after infection (**Fig. 5c** and **Supplementary Video 3**). After compensating for cell movements, we found that intranuclear complexes showed very slow and diffuse movements (movement IV), with an average speed of $0.003 \pm 0.0003 \mu\text{m/s}$ (47 measurements). We found the diffusion coefficient (D) to be between 5×10^{-5} and $2.2 \times 10^{-4} \mu\text{m}^2/\text{s}$ for diffuse intranuclear movements (after fit with $\Delta r^2 = 2nD\Delta t$, where n is the dimension 3). We very occasionally observed the sudden disappearance of the fluorescence of intranuclear HIV-1 complexes, which was apparently not the result of departure from the acquisition field (**Supplementary Video 6** online). We speculate that this disappearance of intranuclear signal could be the consequence of integration followed by repair and association of the HIV-1 integrated proviral DNA with cellular histones.

DISCUSSION

FLAsH labeling of HIV-1 integrase allowed, by virtue of the specific association of integrase with viral DNA, the sensitive detection of both intracytoplasmic reverse-transcription complexes and intranuclear preintegration complexes (PICs). The combination of real-time imaging with quantitative automated 4D dot tracking enabled us to determine for the first time the precise dynamic parameters of HIV-1 intracellular movements (**Fig. 6**) and thus uncover several facets of the HIV-1 replication cycle. In the cytoplasm, in 25 independent trajectories, we noted that infectious HIV-1 complexes consistently underwent actin-like movement before docking at the nuclear membrane. Upstream of this, microtubule-directed movements were also invariably followed by slower actin-like displacements before association with the nuclear membrane. Consistently, inhibition of microtubule- and actin-dependent movements resulted in differential accumulation of HIV-1 complexes in the periphery of the cytoplasm and in perinuclear areas, respectively. Taken together, these data strongly suggest that HIV-1 cytoplasmic transport results from successive transitions from fast microtubule-directed movement to slower actin-mediated movement closer to the nuclear compartment, finally resulting in association with the nuclear membrane. Our results agree with previous results⁶ showing fast microtubule-directed movements toward the nucleus. However, contrary to previous reports⁶, we did not observe a preferential targeting of complexes to the microtubule-organizing center, but rather uniformly distributed complexes all along the

nuclear membrane as would be expected from prior actin-based transport. Whether actin filaments are directly involved in transport upstream of microtubule-directed movements is difficult to assess using this technique, as the vast majority of HIV-1 signal at the immediate postfusion stage results from noninfectious events.

Our ongoing experimentation has led us to hypothesize that the confined vibratory movements exhibited by complexes docked at the nuclear membrane could be accounted for by an interaction with the flexible cytoplasmic filaments of the nuclear pore (data not shown)²⁴ or the dynamic properties of some peripheral nucleoporins²⁵. Studies are currently under way to understand how the HIV-1 PIC, a 9.7-kb

DNA filament complexed with many PIC-associated proteins, interacts with and crawls through the nuclear pore to reach the cell's chromatin and achieve productive infection.

The observation of intranuclear HIV-1 complexes revealed entirely different kinetic parameters compared with cytoplasmic complexes. Indeed, PICs showed only restrained diffuse movement within the nucleus, which could be indicative of interactions with chromatin. We did not observe a special preference for localization of HIV-1 complexes within the nuclear compartment. The fact that intranuclear complexes were relatively rare leads us to believe that integration probably occurs rapidly after entry into the nuclear compartment.

The quantitative multidimensional microscopy approach presented here is expected to contribute to the understanding of the action of cellular factors that cooperate with or restrict HIV-1 infection. It also provides a potentially powerful tool for screening of anti-HIV-1 drugs and optimization of lentiviral gene-transfer vectors.

Our work is the first demonstration of the applicability of the tetracycline-FLAsH labeling technique¹⁵ to an infectious virus. The combination of tetracycline labeling and automatic analysis of kinetic parameters using our 4D particle tracking software should find applications among a large variety of microorganisms.

METHODS

Production of viruses and vectors. We produced pseudotyped HIV_{LAI}(vsv) and HIV_{LAI}(vsv)IN-C4 (tetracycline-tagged) viruses by transient transfection of 293T cells by calcium phosphate coprecipitation with the proviral plasmids deleted in the *env* gene and a VSV-G envelope expression plasmid (pHCMV-G)²⁶. We measured virus production by quantification of p24 viral antigen in the cell supernatants (Perkin Elmer) 48 h after transfection and assayed virus infectivity in a single-cycle titration assay using P4 indicator cells (HeLa CD4 LTR-LacZ)²⁷. The TRIP-CAG-H2B-mRFP lentiviral vector was a generous gift from S. Tajbakhsh (Institut Pasteur). We constructed the TRIP-CMV-CC1 lentiviral vector from pDsRed-N1-p150^{217–548} (kind gift from T.A. Schroer, Johns Hopkins University) after amplification of *CC1* by PCR (see **Supplementary Methods** online) and insertion in a multiple cloning site downstream of a CMV promoter. We produced lentiviral vectors by transient transfection of 293T cells with the vector plasmid, encapsidation plasmid (p8.7) and VSV envelope

expression plasmid as previously described²⁸. We transduced P4 cells with supernatants containing vector particles (1 μg per 10^6 cells) in the presence of 20 $\mu\text{g}/\text{ml}$ of DEAE-dextran and confirmed successful transduction more than 1 week after transduction by fluorescence microscopy for H2B-mRFP expression and PCR for presence of the *CC1* transgene.

FLAsH labeling of viruses and infection. We labeled viral supernatants (at a p24 capsid concentration of 1–2 $\mu\text{g}/\text{ml}$) at room temperature with 0.5 μM FLAsH-EDT2 (FLAsH bis-ethanedithiol; Invitrogen), 1 mM β -mercaptoethanol, 1 mM tris(2-carboxyethyl)phosphine and 1 mM EDT in a total volume of 1 ml, according to the manufacturer's recommendations. For control labeling reactions, we replaced the viral supernatants with serum-free medium. After 2 h, we ultracentrifuged the reactions at 110,000g for 30 min to eliminate unbound FLAsH substrate and then resuspended the pellets in PBS. We quantified the ultracentrifuged viruses using a p24 ELISA assay (Perkin Elmer) and assessed FLAsH incorporation by spectrofluorescence at 485–570 nm using a microplate fluorimeter (Victor, Perkin Elmer). We normalized the labeled viruses at 4 ng of p24 per μl before infection and infected P4 cells with 120 ng (p24 capsid) of FLAsH-labeled virus for 1–2 h at 37 °C.

Virus titrations. We performed one-cycle titration of viruses in triplicate by infecting P4 cells plated in 96-well plates with equivalent amounts of viral particles (2, 1 or 0.5 ng of p24 viral antigen per well). We then measured the β -galactosidase activity 48 h after infection, at which time point signal is imputable to a unique replicative event, using a chemiluminescent β -galactosidase reporter gene assay (Roche) and a microplate fluorimeter.

Confocal fluorescence microscopy. For detection of FLAsH-labeled HIV-1 particles on cover slips, viruses were labeled with FLAsH, ultracentrifuged, spread onto poly-L-lysine-coated cover slips, fixed in 4% paraformaldehyde and permeabilized in 0.5% Triton X-100. For the detection of fluorescent viral particles in fixed cells, P4 cells were cultured and infected on glass cover slips. Twenty-four hours after infection, cells were fixed, permeabilized and mounted in the presence of DAPI (1.5 $\mu\text{g}/\text{ml}$; Vector Laboratories). Images of viral particles on cover slips or fixed cells were acquired using an Apotome (Carl Zeiss) structured illumination fluorescence imaging system mounted on an Axioplan 2 imaging microscope equipped with a Plan-Apochromat $\times 63$ NA-1.4 oil objective and an MRm charge-coupled device camera piloted by AxioVision software. We detected p24 Gag capsid proteins using mouse monoclonal antibodies p25e (clone 157-20; Laboratoire d'Ingenierie des Anticorps, Institut Pasteur) and 183-H12-5C (AIDS Reagent Program) and Cy3-labeled goat antibody to mouse IgG (Amersham Pharmacia). We labeled actin filaments with a phalloidin-TRITC conjugate (Sigma) and microtubules with a monoclonal antibody to α -tubulin (Sigma) followed by Cy3-labeled anti-mouse secondary antibody.

To observe FLAsH-labeled viruses within living cells, we cultured P4 cells on glass-bottomed dishes (#1.5; MatTek) and infected them with FLAsH-labeled virus. For real-time acquisitions, we maintained cells at 37 °C (Bioprotechs) and observed them using spinning-disk confocal microscopy (Perkin Elmer) on an Axiovert 200 microscope equipped with a $\times 100$ NA-1.3 oil Plan-Neofluar

objective lens (Carl Zeiss). We visualized the nuclear compartment by stable transduction with a lentiviral vector (TRIP-CAG-H2B-mRFP) encoding an H2B-mRFP fusion protein and acidified endocytic compartments by staining with the acidotropic probe Red-DAMP (Molecular Probes) according to the manufacturer's instructions.

Computer vision program for automated 4D particle tracking.

We carried out all tracking analyses using an in-house-developed program specifically designed to overcome the limitations of standard tracking programs. Conventional multiple-particle tracking methods are based on simple intensity thresholding, local maxima extraction or template matching to detect spots, and on nearest-neighbor association to perform tracking. These methods work well on image sequences containing only a limited number of very bright spots on a uniform background but are not adapted to tracking biological objects with nonuniform fluorescence intensities on a noisy background and where particle density can be high.

The 4D multitarget tracking method presented here is fully automated and relies on multiscale detection¹⁷, bayesian filtering¹⁸ and robust data association²⁹ to assess the evolution of 3D position, volume and intensity for each HIV-1 intracellular complex. The whole procedure is performed within a bayesian framework¹⁸ in which each object is represented by a state vector that evolves according to biologically realistic dynamic models. Briefly, tracking is composed of three steps at each time frame. First, the HIV-1 complexes are detected in the image stacks using a procedure based on a 3D wavelet transform, which is robust to variations of intensity and to imaging noise¹⁷. Second, an interacting multiple-model filter with three movement models (random motion, constant speed and constant acceleration) allows the prediction of a complex's new position based on its past positions and associates measurements into tracks on the basis of maximum likelihood. The interacting multiple model is an algorithm based on a Markov switching mechanism that allows several *a priori* models to compete with each other to give accurate predictions and estimations of the object states. Finally, the data association step is based on a split-and-merge mechanism that allows the continued tracking of particles even when they merge or separate into smaller entities³⁰.

We subtracted the movement of the cell nucleus from that of HIV-1 complexes associated with the nuclear compartment using the method above to track the center of mass of the nucleus. We detected the nucleus using a 3D gaussian filter followed by automatic thresholding. We assessed the prediction, association and positioning errors of our algorithm from experiments performed with synthetic data²⁹. The calculated positioning error ($\Delta x = \Delta y = 0.0185 \pm 0.0125 \mu\text{m}$; $\Delta z = 0.146 \pm 0.065 \mu\text{m}$) is below the resolutions in x , y (0.129 μm) and z (0.3–0.8 μm) of our real-time acquisitions. The program successfully tracked all the particles in the data sets.

Additional methods. A description of cell culture conditions and DNA constructs is available in **Supplementary Methods**.

Note: Supplementary information is available on the Nature Methods website.

ACKNOWLEDGMENTS

We thank P. Roux for assistance with the Perkin Elmer microscope. N.A. and A.G. were supported by grants from the ANRS AC-14-2 and the Institut Pasteur.

AUTHOR CONTRIBUTIONS

N.A., acquisition, analysis and interpretation of data, and writing of manuscript; A.G., data analysis; K.-A.K., S.M. and E.P., technical help; J.-C.O.-M., data analysis and revision of manuscript; S.S., conception and design of study; P.C., conception and design of study, project supervision and writing of manuscript.

COMPETING INTERESTS STATEMENT

The authors declare that they have no competing financial interests.

Published online at <http://www.nature.com/naturemethods/>
Reprints and permissions information is available online at
<http://npg.nature.com/reprintsandpermissions/>

- Suomalainen, M. *et al.* Microtubule-dependent plus- and minus end-directed motilities are competing processes for nuclear targeting of adenovirus. *J. Cell Biol.* **144**, 657–672 (1999).
- Seisenberger, G. *et al.* Real-time single-molecule imaging of the infection pathway of an adeno-associated virus. *Science* **294**, 1929–1932 (2001).
- Pelkmans, L., Kartenbeck, J. & Helenius, A. Caveolar endocytosis of simian virus 40 reveals a new two-step vesicular-transport pathway to the ER. *Nat. Cell Biol.* **3**, 473–483 (2001).
- Lakadamyali, M., Rust, M.J., Babcock, H.P. & Zhuang, X. Visualizing infection of individual influenza viruses. *Proc. Natl. Acad. Sci. USA* **100**, 9280–9285 (2003).
- Rietdorf, J. *et al.* Kinesin-dependent movement on microtubules precedes actin-based motility of vaccinia virus. *Nat. Cell Biol.* **3**, 992–1000 (2001).
- McDonald, D. *et al.* Visualization of the intracellular behavior of HIV in living cells. *J. Cell Biol.* **159**, 441–452 (2002).
- McDonald, D. *et al.* Recruitment of HIV and its receptors to dendritic cell-T cell junctions. *Science* **300**, 1295–1297 (2003).
- Müller, B. *et al.* Construction and characterization of a fluorescently labeled infectious human immunodeficiency virus type 1 derivative. *J. Virol.* **78**, 10803–10813 (2004).
- Rudner, L. *et al.* Dynamic fluorescent imaging of human immunodeficiency virus type 1 gag in live cells by biarsenical labeling. *J. Virol.* **79**, 4055–4065 (2005).
- Engelman, A., Englund, G., Orenstein, J.M., Martin, M.A. & Craigie, R. Multiple effects of mutations in human immunodeficiency virus type 1 integrase on viral replication. *J. Virol.* **69**, 2729–2736 (1995).
- Smith, D.A. & Simmons, R.M. Models of motor-assisted transport of intracellular particles. *Biophys. J.* **80**, 45–68 (2001).
- Apodaca, G. Endocytic traffic in polarized epithelial cells: role of the actin and microtubule cytoskeleton. *Traffic* **2**, 149–159 (2001).
- Carter, G.C. Vaccinia virus cores are transported on microtubules. *J. Gen. Virol.* **84**, 2443–2458 (2003).
- Leopold, P.L. Dynein- and microtubule-mediated translocation of adenovirus serotype 5 occurs after endosomal lysis. *Hum. Gene Ther.* **11**, 151–165 (2000).
- Griffin, B.A., Adams, S.R. & Tsien, R.Y. Specific covalent labeling of recombinant protein molecules inside live cells. *Science* **281**, 269–272 (1998).
- Maréchal, V., Clavel, F., Heard, J.M. & Schwartz, O. Cytosolic Gag p24 as an index of productive entry of human immunodeficiency type I. *J. Virol.* **72**, 2208–2212 (1998).
- Olivo-Marín, J.C. Extraction of spots in biological images using multiscale products. *Pattern Recognit.* **35**, 1989 (2002).
- Genovesio, A. *et al.* Multiple particle tracking in 3-D+t microscopy: method and application to the tracking of endocytosed quantum dots. *IEEE Trans. Image Process.* **15**, 1062–1070 (2006).
- Quintyne, N.J. *et al.* Dynactin is required for microtubule anchoring at centrosomes. *J. Cell Biol.* **147**, 321–334 (1999).
- Campbell, E.M., Nunez, R. & Hope, T.J. Disruption of the actin cytoskeleton can complement the ability of Nef to enhance human immunodeficiency virus type 1 infectivity. *J. Virol.* **78**, 5745–5755 (2004).
- Zennou, V. *et al.* HIV-1 genome nuclear import is mediated by a central DNA flap. *Cell* **101**, 173–185 (2000).
- Barbosa, P., Charneau, P., Dumey, N. & Clavel, F. Kinetic analysis of HIV-1 early replicative steps in a coculture system. *AIDS Res. Hum. Retroviruses* **10**, 53–59 (1994).
- Farnet, C.M. & Haseltine, W.A. Determination of viral proteins present in the human immunodeficiency virus type 1 preintegration complex. *J. Virol.* **65**, 1910–1915 (1991).
- Rutherford, S.A., Goldberg, M.W. & Allen, T.D. Three-dimensional visualization of the route of protein import: the role of nuclear pore complex substructures. *Exp. Cell Res.* **232**, 146–160 (1997).
- Rabut, G., Doye, V. & Ellenberg, J. Mapping the dynamic organization of the nuclear pore complex inside single living cells. *Nat. Cell Biol.* **6**, 1114–1121 (2004).
- Yee, J.K. A general method for the generation of high-titer, pantropic retroviral vectors: highly efficient infection of primary hepatocytes. *Proc. Natl. Acad. Sci. USA* **91**, 9564–9568 (1994).
- Charneau, P. *et al.* HIV-1 reverse transcription. A termination step at the center of the genome. *J. Mol. Biol.* **241**, 651–662 (1994).
- Naldini, L. *et al.* In vivo gene delivery and stable transduction of nondividing cells by a lentiviral vector. *Science* **272**, 263–267 (1996).
- Genovesio, A. & Olivo-Marín, J.C. Split and merge data association filter for dense multi-target tracking. *IEEE ICPR'04* **4**, 677–680 (2004).